AIAA JOURNAL
Vol. 33, No. 8, August 1995

Compressible Cavity Flow Oscillation due to Shear Layer Instabilities and Pressure Feedback

Xin Zhang*
University of Southampton, Southampton SO17 1BJ, England, United Kingdom

A computational analysis was performed on a compressible flow oscillation due to shear layer instabilities over a cavity and pressure feedback in a cavity of length-to-depth ratio 3 at Mach 1.5 and 2.5. The mass-averaged Navier–Stokes equations were solved. Turbulence closure was achieved using a k–ω model with compressibility corrections. Self-sustained oscillations were produced. Negative form drag coefficient was observed within an oscillatory cycle due to mass ejection from the cavity near the trailing edge and vortex production near the leading edge. The shock wave-expansion wave interaction patterns, modes of the oscillation, sound pressure level, and time-averaged surface pressure were compared with experimental results of previous investigations and good agreement was achieved, particularly the time-averaged pressure. The prediction showed a marked improvement over earlier analysis.

Nomenclature

a	= speed of sound
C_d	= form drag coefficient, $\int_{-1}^{0} 2(p_{\text{downstream face}} - p_{\text{upstream face}})/\rho_\infty V_\infty^2 \cdot \mathrm{d}y$
D	= depth of cavity
e_t	= total energy, $p/(\gamma - 1) + \rho(u_x^2 + u_y^2)/2$
k	= kinetic energy of turbulent fluctuations per unit mass
L	= length of cavity
l	= turbulence length scale
M	= Mach number
Pr	= Prandtl number, 0.72
Pr_t	= turbulent Prandtl number, 0.9
p	= pressure
q	= heat flux
Re	= Reynolds number, $\tilde{\rho}_\infty \tilde{V}_\infty D/\tilde{\mu}_\infty$
T	= temperature
t	= normalized time
u_x, u_y	= velocity components
V	= local flow velocity
X, Y	= dimensional Cartesian coordinates
x, y	= normalized Cartesian coordinates, X/D and Y/D
γ	= specific heat ratio, 1.4
$\Delta x, \Delta y$	= computational cell sizes
δ	= boundary-layer thickness at $0.99V_\infty$
μ	= viscosity
μ_l	= molecular viscosity
μ_t	= turbulent eddy viscosity
ρ	= density
τ	= Reynolds stress
ω	= specific dissipation rate, $\sqrt{k}/l$

Subscripts

∞	= freestream condition
rms	= root-mean-square value

Superscript

$\sim$	= dimensional variable

Received June 11, 1994; revision received Oct. 31, 1994; accepted for publication Nov. 12, 1994.

*Lecturer, Department of Aeronautics and Astronautics. Member AIAA.

I. Introduction

COMPRESSIBLE flow oscillations over geometries such as groove, cavity, and cutout have been studied in the past using experimental techniques and more recently through numerical computation. Traditionally, experimental research focuses on internal store release, wheel well acoustics, and pitching motions due to surface pressure variations. Transient surface pressure is also measured to determine the tones and their likely effects on structure. Computations have been performed to study salient features and to provide insight into physics. The existence of a number of complex flow phenomena in the flowfield also sustained interest over the years and continues to stimulate further research. These include boundary-layer separation, shear layer instability, vortex flow, acoustic radiation, and shock/expansion wave interaction. The presence of these complex mechanisms could lead to changes in pressure, noise, and convective heat transfer environment. It also introduces difficulties in performing reliable and accurate measurement inside the flowfield. Intrusive measurement methods are likely to alter the unsteady flow environment. Some reliable information, though, can be obtained through surface pressure tapping, pressure transducer measurement, and optical methods such as holographic interferometry. Apart from experimental and computational studies, there have been a number of attempts in studying the unsteady flow analytically. The scope for analytical study, though, is limited. Important physics are often lost when simplifying assumptions are made, and so far only the flow oscillatory frequency can be confidently predicted with empirical input. To achieve a better understanding of the physics and to be able to predict the flow reliably, it is important to undertake research using both experimental and theoretical (analytical and numerical) methods.

The general focus of this research is compressible flow past a cavity (or groove). Figure 1 gives a schematic of the geometry. A boundary layer is developed on the surface approaching the cavity. It separates to form a shear layer at the leading edge of the cavity. Depending on a number of flow parameters, among them L/D, δ, M_∞, and Re, the shear layer will either reattach to the downstream face $b5$ (open cavity) or the flow $b4$ (closed cavity). An open cavity flow normally occurs at $L/D \leq 10$ and a closed cavity flow at $L/D > 10$. There are perhaps other transitional states. A closed cavity flow is often steady. Its surface pressure distribution could be detrimental to performance such as heat transfer. An open cavity flow is susceptible to instabilities of the shear layer and is likely to be unsteady. As a result, there could be intensive noise radiation and large shock motion in the flowfield. Experimental studies initiated research in the subject.[1–7] There are also some analytical studies. Tam and Block[8] analyzed the coupling between the shear layer instabilities and the acoustic feedback. The method was applied to supersonic flow and to a thick shear layer with empirical parameter

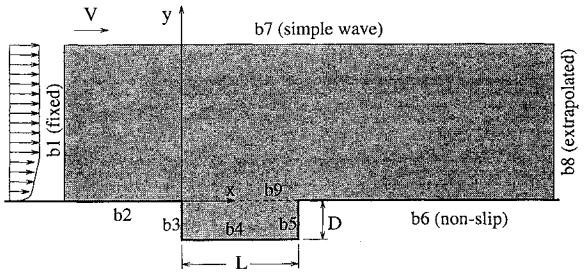

Fig. 1 Schematic of the geometry.

input.[7] The method of Tam and Block provides some clues as to the shift in the dominant mode of oscillation but not quantitative predictions of the shift.

Computational analysis has been performed on the flow, which is particularly useful when used in conjunction with experiments. Among many researchers, Hankey and Shang[9] studied an $L/D = 2.25$ cavity flow at $M_\infty = 1.5$, $Re = 5.2 \times 10^5$. Two-dimensional compressible Navier–Stokes equations were solved using the MacCormack scheme. Turbulence closure was achieved using the Cebeci–Smith model. Rizzetta[10] analyzed a three-dimensional compressible flow over an $L/D = 5.07$ cavity at $M_\infty = 1.5$ and $Re = 2.1 \times 10^5$. The width-to-depth ratio W/D of the cavity was 2.67. Turbulence was simulated using the Baldwin–Lomax model. The treatment of turbulence was two-dimensional and the results showed a predominantly two-dimensional flowfield. The MacCormack scheme was also employed in solving the governing equations. Zhang and Edwards[11] studied $M_\infty = 1.5$ and 2.5 flows over an $L/D = 3$ cavity at $Re = 4.5 \times 10^5$ using a scheme developed by Brailovskaya.[12] An eddy-viscosity model due to Deiwert[13] was employed. In all of these studies, the idea of relaxation length was applied to the turbulence model to account for the downstream effects of turbulence. These studies and others as well could be useful when performed with proper experimental backing. For example, all of them showed the interaction of shear layer driven vortices inside the cavity. When viewed together with either schlieren pictures or interferograms they provided plausible explanations of the oscillation mechanisms. There were major shortcomings, though, in many of these approaches. The time-averaged surface pressure field was often not satisfactorily estimated. As a result, predictions of cavity drag and pitching motion variations still mainly relied on wind-tunnel experimentation. Because of the numerical schemes used and inadequate computational grid cell size above the cavity, shock/expansion wave interaction was either not resolved accurately or not resolved at all. This poses serious problems when attempting to calculate noise radiation from the cavity. There could be a number of causes. Shock waves in the flowfield are difficult to resolve using a finite difference scheme with artificial damping. There is a major question mark on the application of a zero-equation turbulence model to the cavity flow. Its application as well as that of the relaxation length is often done on an ad hoc basis. An important factor in determining the pressure environment inside the cavity, and consequently that outside of the cavity, is the shear layer impingement. If the effects of the turbulent mixing are not properly addressed, the prediction of the pressure field is difficult to achieve. It is, thus, not surprising to find poor predictions of the pressure field and the dominant oscillatory modes.

The specific focus of the present study is to investigate a turbulent flow over an open cavity at supersonic speeds. Attention is focused on three areas: 1) time-averaged surface pressure for a better cavity drag estimation, 2) narrow-band tones, and 3) shock wave and expansion wave interaction for noise radiation prediction. A wind-tunnel test case documented by Zhang and Edwards[7] is chosen in the study (see Sec. II.C, Flow Conditions). Time-averaged surface pressure, time-dependent surface pressure, spark schlieren records, and holographic interferograms are available for comparison.

II. Details of Analysis

A. Governing Equations

We consider a turbulent compressible flowfield governed by the following conservative laws written in a Cartesian coordinate (x, y) system:

$$\frac{\partial}{\partial t}\begin{pmatrix}\rho\\ \rho u_x\\ \rho u_y\\ e_t\end{pmatrix}+\frac{\partial}{\partial x}\begin{pmatrix}\rho u_x\\ \rho u_x^2+p\\ \rho u_x u_y\\ (e_t+p)u_x\end{pmatrix}+\frac{\partial}{\partial y}\begin{pmatrix}\rho u_y\\ \rho u_x u_y\\ \rho u_y^2+p\\ (e_t+p)u_y\end{pmatrix}$$
$$=\frac{\partial}{\partial x}\begin{pmatrix}0\\ \tau_{xx}\\ \tau_{xy}\\ u_x\tau_{xx}+u_y\tau_{xy}+q_x\end{pmatrix}+\frac{\partial}{\partial y}\begin{pmatrix}0\\ \tau_{xy}\\ \tau_{yy}\\ u_x\tau_{xy}+u_y\tau_{yy}+q_y\end{pmatrix} \tag{1}$$

Normalized variables are used in Eq. (1) and will be used in the following expressions. Length is normalized by D, density by $\tilde{\rho}_\infty$, velocity by $\tilde{V}_\infty$, temperature by $\tilde{T}_\infty$, pressure and total energy by $\tilde{\rho}_\infty \tilde{V}_\infty^2$, time by $D/\tilde{V}_\infty$, and viscosity by $\tilde{\mu}_\infty$.

The relation between the T, p, and ρ is given by the state equation $p = \rho T/(\gamma M_\infty^2)$. The stress terms are

$$\tau_{xx} = \frac{2}{3}\frac{\mu_l+\mu_t}{Re}\left(2\frac{\partial u_x}{\partial x}-\frac{\partial u_y}{\partial y}\right)$$
$$\tau_{xy} = \frac{\mu_l+\mu_t}{Re}\left(\frac{\partial u_x}{\partial y}+\frac{\partial u_y}{\partial x}\right) \tag{2}$$
$$\tau_{yy} = \frac{2}{3}\frac{\mu_l+\mu_t}{Re}\left(2\frac{\partial u_y}{\partial y}-\frac{\partial u_x}{\partial x}\right)$$

and the heat flux terms are

$$q_x = \frac{1}{(\gamma-1)M_\infty^2 Re}\left(\frac{\mu_l}{Pr}+\frac{\mu_t}{Pr_t}\right)\frac{\partial T}{\partial x}$$
$$q_y = \frac{1}{(\gamma-1)M_\infty^2 Re}\left(\frac{\mu_l}{Pr}+\frac{\mu_t}{Pr_t}\right)\frac{\partial T}{\partial y} \tag{3}$$

The molecular viscosity μ_l is calculated using Sutherland's law:

$$\mu_l = T^{1.5}\left(\frac{1+110.4/\tilde{T}_\infty}{T+110.4/\tilde{T}_\infty}\right) \tag{4}$$

B. Turbulence Model

A k–ω turbulence model due to Wilcox[14] is used to calculate the turbulent eddy viscosity μ_t. The governing equations for the turbulent kinetic energy k and the specific dissipation rate ω are

$$\frac{\partial \rho k}{\partial t}+\frac{\partial \rho u_x k}{\partial x}+\frac{\partial \rho u_y k}{\partial y} = \sigma_{xt}\frac{\partial u_x}{\partial x}+\tau_{xyt}\left(\frac{\partial u_x}{\partial y}+\frac{\partial u_y}{\partial x}\right)$$
$$+\sigma_{yt}\frac{\partial u_y}{\partial y}-Re\beta_i^*\rho k\omega+\frac{\partial}{\partial x}\left(\frac{(\mu_l+\sigma^*\mu_t)}{Re}\frac{\partial k}{\partial x}\right)$$
$$+\frac{\partial}{\partial y}\left(\frac{(\mu_l+\sigma^*\mu_t)}{Re}\frac{\partial k}{\partial y}\right) \tag{5}$$

$$\frac{\partial \rho\omega}{\partial t}+\frac{\partial \rho u_x\omega}{\partial x}+\frac{\partial \rho u_y\omega}{\partial y}$$
$$=\alpha\frac{\omega}{k}\left[\sigma_{xt}\frac{\partial u_x}{\partial x}+\tau_{xyt}\left(\frac{\partial u_x}{\partial y}+\frac{\partial u_y}{\partial x}\right)+\sigma_{yt}\frac{\partial u_y}{\partial y}\right]-Re\beta_i\rho\omega^2$$
$$+\frac{\partial}{\partial x}\left(\frac{(\mu_l+\sigma\mu_t)}{Re}\frac{\partial\omega}{\partial x}\right)+\frac{\partial}{\partial y}\left(\frac{(\mu_l+\sigma\mu_t)}{Re}\frac{\partial\omega}{\partial y}\right) \tag{6}$$

where k is normalized by $\tilde{V}_\infty^2$ and ω by $\tilde{\rho}\tilde{V}_\infty^2/\tilde{\mu}_\infty$. Assuming the

Boussinesq approximation is valid, the Reynolds stress terms in Eqs. (5) and (6) are

$$\sigma_{xt} = \frac{2}{3}\frac{\mu_t}{Re}\left(2\frac{\partial u_x}{\partial x} - \frac{\partial u_y}{\partial y}\right) - \frac{2}{3}\rho k$$

$$\tau_{xyt} = \frac{\mu_t}{Re}\left(\frac{\partial u_x}{\partial y} + \frac{\partial u_y}{\partial x}\right) \tag{7}$$

$$\sigma_{yt} = \frac{2}{3}\frac{\mu_t}{Re}\left(2\frac{\partial u_y}{\partial y} - \frac{\partial u_x}{\partial x}\right) - \frac{2}{3}\rho k$$

The turbulent eddy-viscosity is given by $\mu_t = \rho k/\omega$. The closure constants in the k–ω equations are $\alpha = 5/9$, $\beta_i = 3/40$, $\beta_i^* = 9/100$, $\sigma = 1/2$, and $\sigma^* = 1/2$. Equations (5) and (6) are modified for the effects of compressibility. The modification and details can be found in Wilcox.[15]

C. Flow Conditions

The test cases selected are two-dimensional cavity flows driven by a turbulent shear layer (Fig. 1). The depth of the cavity is 15 mm and the lengths are 45 mm. At $M_\infty = 1.5$, the freestream air temperature $\tilde{T}_\infty$ is 200 K and static pressure $\tilde{p}_\infty$ is 53801.7 psia. The oncoming boundary layer has a thickness $\tilde{\delta}$ of 5 mm, a displacement thickness $\tilde{\delta}^*$ of 0.929 mm, and a momentum thickness $\tilde{\theta}$ of 0.417 mm. The skin friction coefficient C_f is 2.05×10^{-3}. At $M_\infty = 2.5$, the respective values are 128.9 K, 12390.7 psia, 5 mm, 0.328 mm, 1.29 mm, and 1.79×10^{-3}. In the computation, freestream values of $\tilde{k}$ and $\tilde{\omega}$ are 1.258 m^2/s^2 and $2.567 \times 10^4/s^{-1}$ at $M_\infty = 1.5$, and 1.912 m^2/s^2 and 3.503×10^4 s^{-1} at $M_\infty = 2.5$, respectively. In experiments, the width of the test model is 114 mm and the flow remains basically two-dimensional. The geometry considered here is "open."[2,3]

D. Numerical Algorithm, Grid, and Validation

To preserve conservation under the present numerical scheme, a structured grid of rectangles is used. These form the control volumes for the application of the conservation laws. The Roe flux difference split approximate Riemann solver[16] is used to evaluate the inviscid fluxes on the cell surfaces. A second-order extension is implemented.[17,18] The integration is performed in operator-split form.[19] An "entropy fix" is employed to achieve the "entropy satisfying" condition.[20,21] Implementation of the k–ω equations into the scheme follows the same procedures described by Roe[16] and will not be repeated here. To preserve monotonicity the min-mod flux limiter is used. The viscous stress and heat fluxes are calculated from the application of the Gauss theorem. Central difference is used to calculate viscous terms at the cell vertex and at the cell face center.

Along the inlet $b1$, the flow is fixed throughout the computation. The upstream effect of the cavity was found to be limited to one boundary-layer thickness in experiment.[7] The fixed condition is thus believed to be adequate. The turbulent boundary-layer profile is obtained using the EDDYBL program of Wilcox.[22] Along the solid walls ($b2$–$b6$), the nonslip condition applies. The wall temperature T_w is calculated using the adiabatic condition. The relation between the velocity and the surface shear stress u_τ is calculated using the Van Driest compressible law of the wall. Von Kármán constant κ and the wall constant B are 0.41 and 5.0, respectively. Near the solid wall, values of $k(=u_\tau^2/0.3)$ and $\omega[=\sqrt{k}/(0.548\kappa y_t)]$ are updated at every iteration, where y_t is the normal distance between the cell center and the wall. Along the upper boundary $b7$, a simple wave condition ($\partial F/\partial \eta = 0$) is imposed, where F is a conservative variable and η the local outgoing characteristic line along the boundary. The extrapolated condition was used on $b7$, but was found to result in reflections of the moving shock waves into the computational domain. The simple wave condition effectively eliminated the reflection. Along the outlet $b8$, the conservative variables are extrapolated along the streamwise direction by assuming zero transverse velocity component. For the oscillatory flowfield, there will always upstream disturbances convected within the boundary layer. The effect is difficult to quantify. In this study, $b8$ is placed at $x = 9$.

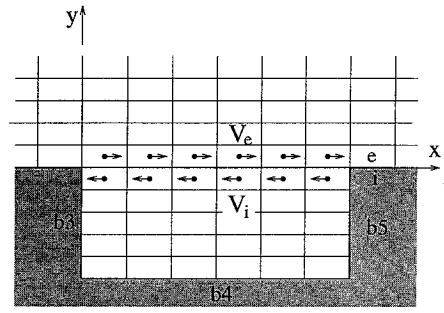

Fig. 2 Schematic of the initial flow condition on the open face of the cavity.

At the beginning of the computation, the initial flow condition on $b1$ is imposed on the flowfield above the cavity. Inside the cavity below $b9$, two types of initial conditions have been tested. A numerical experiment was performed on an $M_\infty = 1.5$ flow over an $L/D = 1$ cavity using a no-flow condition, where the local flow velocity is set to zero and the temperature and pressure assume the stagnation and the freestream values, respectively. The calculation was found to take a long time to reach a self-sustained oscillatory state (constant p_{rms} and tone frequencies). A typical time scale is $t = 600\, D/\tilde{V}_\infty$. If the computational time step is $0.5\Delta t_{\text{CFL}}$ [Courant–Friedrichs–Lewy (CFL) condition] this necessitates 60,000 iterations for the test case. Instead, a mass source is introduced into the flowfield inside the cavity. The effects are to produce the initial disturbances for the onset of the feedback mechanism at the trailing edge or on the downstream face of the cavity. Assuming the cell strip immediately above the cavity along $b9$ is indexed by e and that below the cavity by i (Fig. 2), we have

$$\rho|_i = \rho|_e, \qquad \rho u_x|_i = -\rho u_x|_e, \qquad \rho u_y|_i = -\rho u_y|_e$$

$$e_t|_i = e_t|_e, \qquad \rho k|_i = \rho k|_e, \qquad \rho\omega|_i = \rho\omega|_e$$

Under this condition, the self-sustained oscillatory state can be reached after $t = 100$–$200 D/\tilde{V}_\infty$. The computational domain covers an area between $x = -3$ to 9 and $y = -1$ to 4. Tests were conducted to select a suitable grid which can capture the salient features. Two types of tests were performed: one with a laminar boundary layer and another with a turbulent boundary layer. Both were run under the same external conditions (M_∞, $\tilde{\delta}$, $\tilde{T}_\infty$, and $\tilde{p}_\infty$). The reason for performing the laminar calculation is to obtain a quick assessment of the grid sensitivity. As the flow oscillation is widely believed to be associated with the shear layer instabilities, the test will give an indication of the grid effects. Indeed, all of the laminar cases (see the following description) have the same oscillatory frequency at $f \approx 9660$ Hz at $M_\infty = 2.5$, which is close to the measured value of 10,010 Hz. Three grids were used: 1) $\Delta x = 0.075$ and $\Delta y = 0.04$, 2) $\Delta x = 0.0667$ and $\Delta y = 0.0222$, and 3) $\Delta x = 0.01875$ and Δy 0.01. The pressure histories were recorded at $x = -0.9333, -0.4$ (upstream), 0.333, 2.333 (floor), 3.6, and 5.6 (downstream), and these positions remained fixed for all of the cases. The duration of the calculation was $800 \sim 1000 D/\tilde{V}_\infty$. After about $t = 100$–$200 D/\tilde{V}_\infty$, constant p_{rms} and invariant tone frequencies were observed. For the three grids, the sound pressure levels (SPL) at $x = 2.333$ were 151.48, 161.29, and 162.14 dB, respectively. It was noticeable that the discrepancy was reduced as the grid was refined. Based on the laminar test results, two grids were selected for the turbulent test: a) $\Delta x = 0.075$ and $\Delta y = 0.025$ and b) $\Delta x = 0.0375$ and $\Delta y = 0.0125$. The calculation was run for a duration of at least of $700 D/\tilde{V}_\infty$. This enabled the flow to reach the self-sustained state and provided enough data points for the time domain analysis. Figure 3 shows an example of the predicted surface pressures using the two grids. The influence of the fine grid 2 is mainly on the high-frequency harmonics and is relatively small. There is also a negligible shift in the frequency at $M_\infty = 1.5$ that is not present at $M_\infty = 2.5$. The result suggests that the grids selected are capable of capturing the salient features of the flow, and the resolution is sufficient.

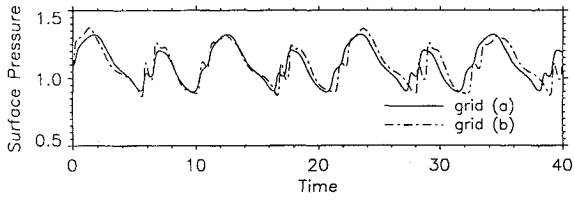

Fig. 3 Surface pressure fluctuation p/p_∞ in the self-sustained state at $x = 0.333$.

Fixed time steps were used in the calculation. The stepping times were set $0.7\Delta t_{\text{CFL}}$ at $M_\infty = 1.5$ and $0.5\Delta t_{\text{CFL}}$ at $M_\infty = 2.5$, respectively. The calculation was done on a Silicon Graphics station.

III. Results and Discussion

A. Self-Sustained Fluid Flow Oscillation Physics

Experiment and stability analysis[7] indicate that the shear layer formed over the cavity is hydrodynamically unstable at Mach 1.5 and 2.5. With a proper combination of L, M, and δ, small disturbances produced by the boundary-layer separation or the external flowfield could be amplified in the shear layer and fed back at the trailing edge (inside the cavity when the external flow is supersonic), resulting in a self-sustained flow oscillation. The first task of the present analysis is, thus, to make sure that a self-sustained oscillation is indeed achieved. This is done by extending the computation time to over $700D/\tilde{V}_\infty$. Figure 4 gives a monitored pressure history on the floor of the cavity. The flow is seen to have reached a self-sustained oscillatory state after about $200D/\tilde{V}_\infty$. Unlike the laminar flow computation where the base mode (first) of the oscillation is either not observed or very weak, base modes at 2651 and 3408 Hz are predicted for the $M_\infty = 1.5$ and $M_\infty = 2.5$ flows, respectively. These values compare well with the measured values of 2645 and 3467 Hz of Ref. 7. At $M_\infty = 1.5$, the first and second modes are closely associated with the production and downstream convection of vortices by the shear layer. At $M_\infty = 2.5$, the third mode is also important (see later sections).

When the flow is oscillatory, unsteady shock waves are produced above the cavity. The interaction and propagation of these shock waves not only generate far-field noise emission but also affect the structural performance of nearby aerodynamic surfaces. Thus, it is important to produce correct shock patterns above the cavity. Figures 5–10 present density contours, Mach number contours, and instantaneous streamlines at four typical states in a complete cycle of oscillation and for the two Mach numbers. The present treatment of the upper computation boundary *b*7 is seen to be adequate in that there is no reflection back into the computation domain. The current computation seems to have captured the dominant physics of the flow oscillation. The wave patterns above the cavity closely resemble the experimentally observed images.[23] These waves are generated through the shear layer deflection, which in turn is associated with the vortex production and convection. Thus, they reflect the modes of the flow oscillation inside the cavity. In Figs. 7 and 10, the instantaneous streamline plots indicate the movement of the shear layer driven vortex inside the cavity. The streamlines are plotted to the edge of the oncoming boundary layer. The shear layer is seen to reattach at the trailing edge of the cavity and a new boundary layer (with a predominantly wake-like structure) is developed. In both the density and the Mach number contour plots, the downstream convection of large vortical structures is visible. This feature is present in experimentally observed images as well. It is conceivable that the cavity will exert a considerable influence on the downstream flowfield through these large structures. Of the four states, states a and c represent mass ejection from the cavity near the trailing edge and production of a vortex by the shear layer near the leading edge. This results in low pressure near the trailing edge and high pressure near the leading edge. The net result is a decrease in the form drag coefficient C_d to a negative value (see Fig. 11). States b and d represent shear layer impingement to the downstream face of the cavity and outward deflection of the shear layer near the leading edge. A high-pressure region is formed near

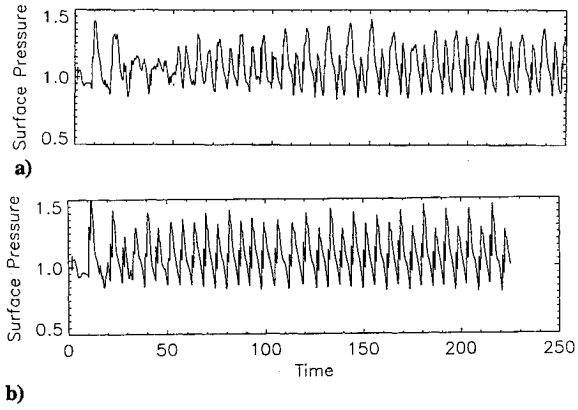

Fig. 4 Monitored pressure histories p/p_∞ on the floor of the cavity: a) $M_\infty = 1.5$ and b) $M_\infty = 2.5$.

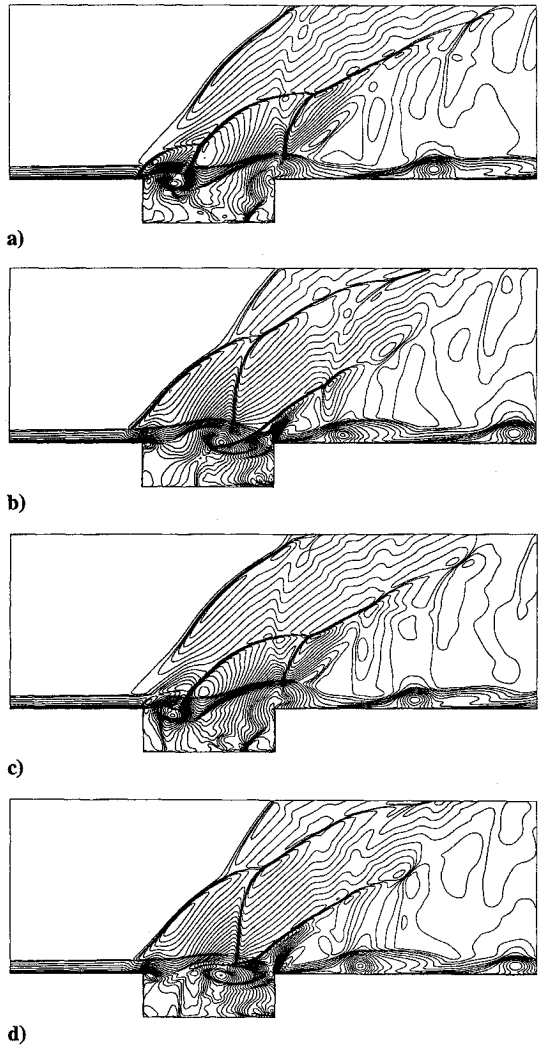

Fig. 5 Density contours at $M_\infty = 1.5$, $\Delta\rho = 0.03$, grid b: a) mass ejection, b) shear layer impingement, c) mass ejection, and d) shear layer impingement.

the trailing edge and a low-pressure region near the leading edge. C_d is at its highest. Overall, the time-averaged effect is to produce a positive value of C_d. The exact behavior of C_d with the cavity geometry and flow conditions is not the subject of this particular study and awaits further investigation.

The variation of C_d is presented in Fig. 11. Different points in a complete cycle of oscillation (corresponding to those in Figs. 5–10) are marked. In Fig. 11, a relative time scale is used. The starting time $t = 0$ represents a point when the flow has arrived at a self-sustained oscillatory state. At $M_\infty = 1.5$, the oscillation is seen to be dominated by the first mode (base mode) and the second mode.

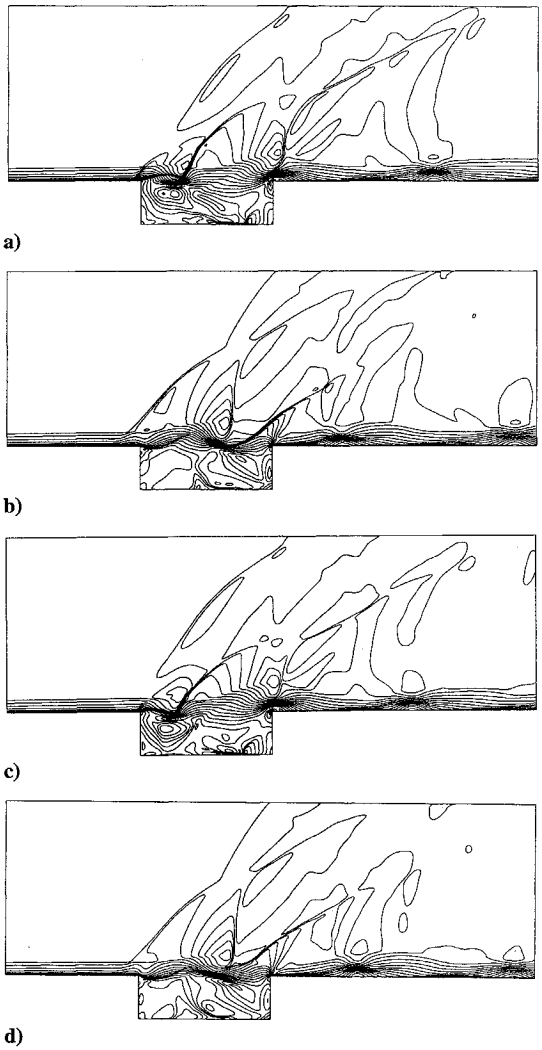

Fig. 6 Mach number contours at $M_\infty = 1.5, \Delta M = 0.1$, grid b: a) mass ejection, b) shear layer impingement, c) mass ejection, and d) shear layer impingement.

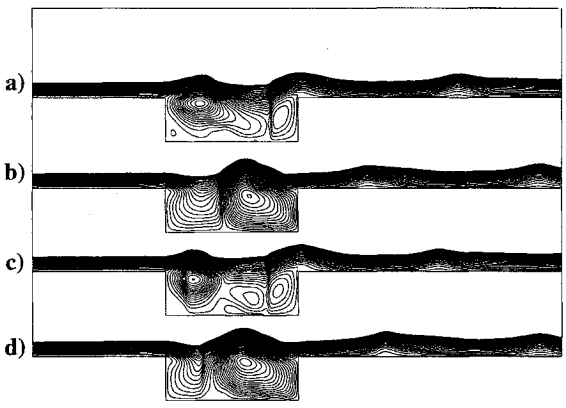

Fig. 7 Instantaneous streamlines at $M_\infty = 1.5$, grid b: a) mass ejection, b) shear layer impingement, c) mass ejection, and d) shear layer impingement.

At $M_\infty = 2.5$, the first two modes are still prominent. The third mode also appears in the form of the slight wiggle between states d and a. The $M_\infty = 1.5$ results agree with the experimental observation. At $M_\infty = 2.5$, the low-frequency harmonics are observed in experiment. However, the predicted dominant mode seems to be the second one. In experimental observation, the second mode dominates at $M_\infty = 1.5$ and the third at $M_\infty = 2.5$. Apart from these low-frequency modes of oscillation which are observed in experiment, high-frequency harmonics are also noticed, particularly inside the cavity (see Fig. 4). This feature will be discussed in the

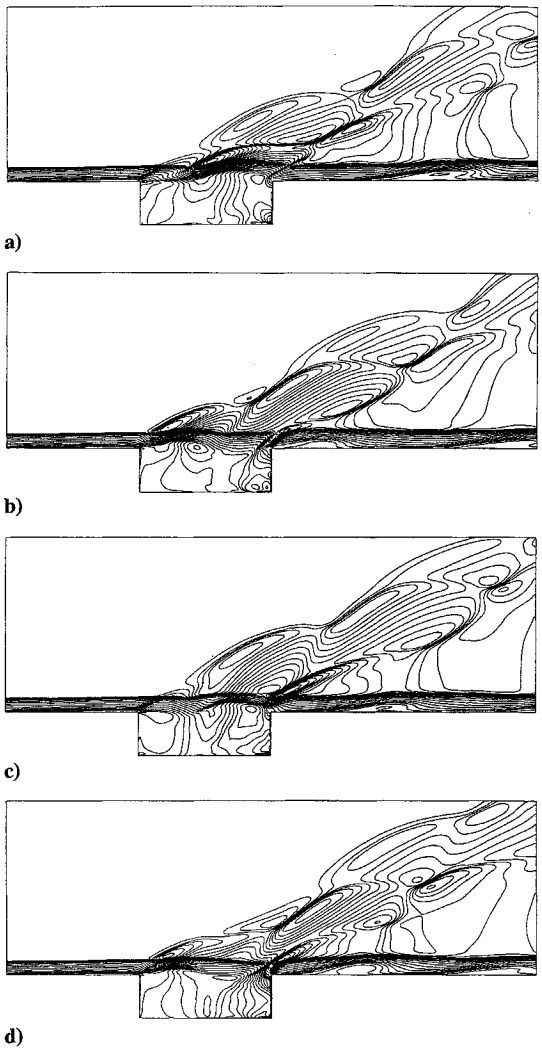

Fig. 8 Density contours at $M_\infty = 2.5, \Delta\rho = 0.03$, grid a: a) mass ejection, b) shear layer impingement, c) mass ejection, and d) shear layer impingement.

next section. In a wind-tunnel experiment, it is difficult to measure the transient behavior of C_d. Yet it is important to understand the physics as in many practical environments the dynamic characteristics may be affected by the presence of a cavity. One way to study the transient behavior is to achieve a good prediction of the time-averaged surface pressure using computational methods. In experiment, the time-averaged surface pressure can be measured with a sufficient degree of confidence through pressure tappings and ensemble averaging. A good agreement between the prediction and the measurement would lend credibility to the transient C_d prediction. This is the approach used in this study.

B. Pressure Fluctuation

To analyze the transient behaviors of the flow power spectral densities (PSDs) of the monitored surface pressures are calculated, and the results are shown in Figs. 12 and 13. The monitoring positions are $x = 0.333$ and 2.333. For the measured data, the cut-off frequencies are 41,667 Hz at $M_\infty = 1.5$ and 50 kHz at $M_\infty = 2.5$. In the computational analysis, the CFL condition restricts the stepping time. As a result, the sampling frequency is quite high (3778–9500 kHz). The monitored data from the computation are decimated at 60 kHz using an eighth-order lowpass Chebyshev type I filter. The cut-off frequency is at 48 kHz. Results between 0–20 KHz are given in Figs. 12 and 13.

In the computational analysis, high-frequency harmonics of the base mode are observed. In the experimental study,[7] the high-frequency harmonics are either of much broader band or suppressed. Two factors could have contributed to this: 1) background noise in

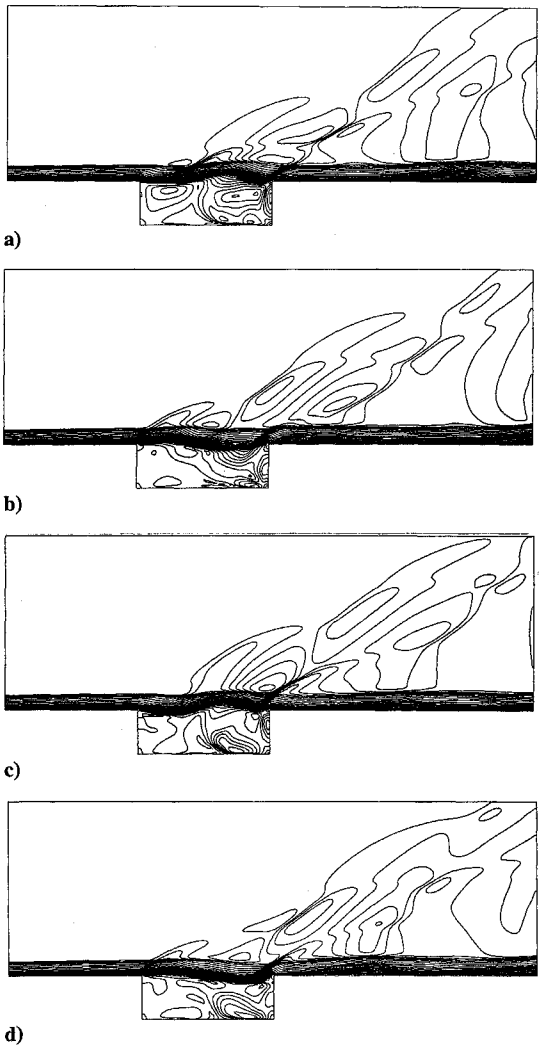

Fig. 9 Mach number contours at $M_\infty = 2.5$, $\Delta M = 0.1$, grid a: a) mass ejection, b) shear layer impingement, c) mass ejection, and d) shear layer impingement.

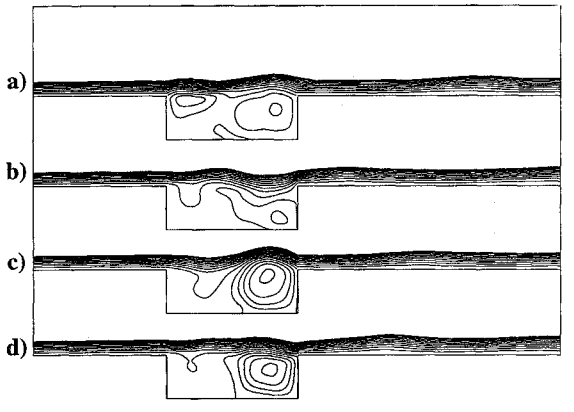

Fig. 10 Instantaneous streamlines at $M_\infty = 2.5$, grid a: a) mass ejection, b) shear layer impingement, c) mass ejection, and d) shear layer impingement.

the wind-tunnel tests and 2) incorrect levels of turbulent mixing in the shear layer in the computation. The existence of the background noise could well have dampened the low-energy high-frequency harmonics. Another cause could be the predicted levels of the turbulent mixing in the shear layer. If they are not predicted correctly, high-frequency components of the spectra could be affected. The observation could be true in that the turbulence model used is known to be sensitive to the freestream value of ω. However, this will lead to an inaccurate flow entrainment prediction. It follows that the shear layer impingement onto the downstream face $b5$ will be affected.

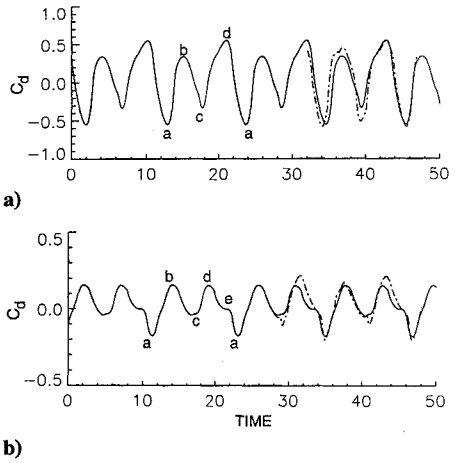

Fig. 11 Form drag coefficient; dotted lines grid b results: a) $M_\infty = 1.5$ and b) $M_\infty = 2.5$.

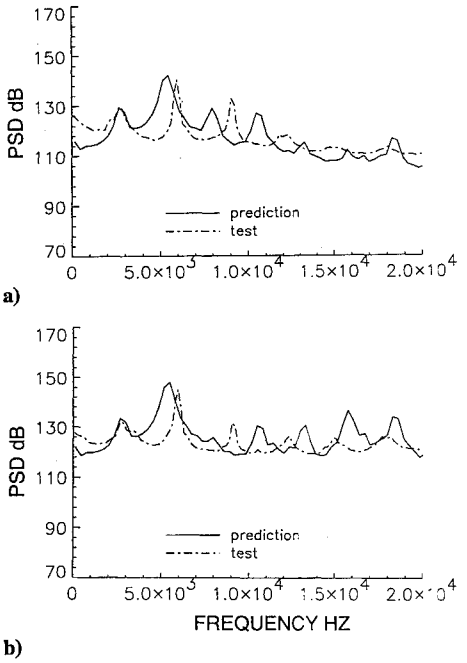

Fig. 12 Power spectral densities on the floor of the cavity at $M_\infty = 1.5$: a) $x = 0.333$ and b) $x = 2.333$.

One would then expect to see significant discrepancies in the time-averaged pressure prediction. The fact that the time-averaged pressure is predicted accurately suggests that the mixing level prediction is not the cause, and the background noise could be the major contributing factor. The computational results obtained in the present study are "clean" in that they are sampled after the self-sustained oscillation is achieved. Thus, there would be no background noise due to the starting up process of the computation. This might explain the differences in the very low-frequency range of the spectra.

Compared to earlier attempts,[9–11] the results just shown give good predictions of the overall levels of the pressure fluctuation, generally within 4 dB of the measured values and the tone frequencies. At $M_\infty = 1.5$, the measured tone frequencies for the first three modes are 2645, 5900, and 9155 Hz, and the predicted values are 2651, 5459, and 10,450 Hz. At $M_\infty = 2.5$, the measured values are 3467, 6787, and 10,010 Hz, and the predicted values are 3408, 6667, and 9927 Hz. The tone frequency prediction is generally good for the majority of the computation attempts, mainly because the frequencies are influenced by the flow velocity, length, and temperature. The difficulty lies in the prediction of the levels of the oscillation. In interpreting the results, caution should be exercised to compare the peak frequency values. They are liable to be affected by a multitude of factors, particularly the decimalization of the high-frequency computational results. A reasonable indicator may be the

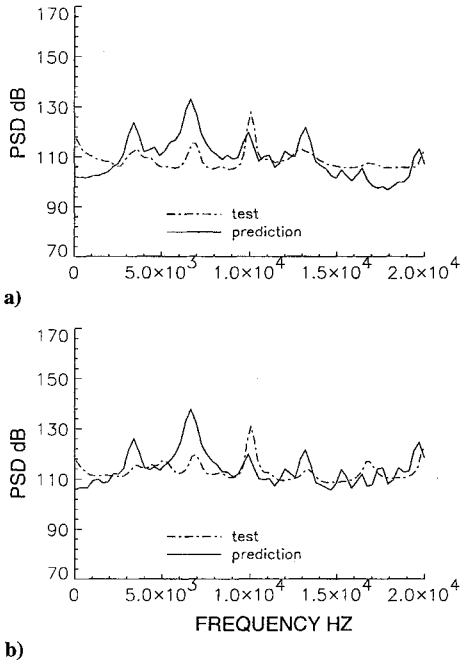

Fig. 13 Power spectral densities on the floor of the cavity at $M_\infty = 2.5$: a) $x = 0.333$ and b) $x = 2.333$.

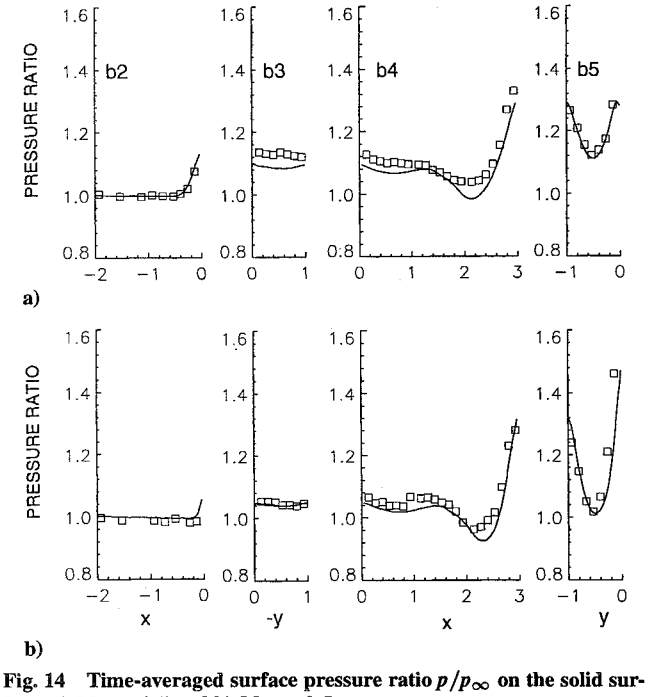

Fig. 14 Time-averaged surface pressure ratio p/p_∞ on the solid surface: a) $M_\infty = 1.5$ and b) $M_\infty = 2.5$.

overall levels of the oscillation. In this study, the predicted overall SPL values at $M_\infty = 1.5$ are 170.8 dB at $x = 0.333$ and 177.0 dB at $x = 2.333$. These compare with the measured values of 166.8 and 171.5 dB. At $M_\infty = 2.5$, the predicted values are 161.4 dB at $x = 0.333$ and 165.8 dB at $x = 2.333$, which compare with the measured values of 155.5 and 159.8 dB. The discrepancies are within 4–6 dB. It shows a marked improvement over the earlier attempts.[9–11] Overall, the $M_\infty = 1.5$ results are better than these at $M_\infty = 2.5$, particularly in terms of the dominant mode which is predicted correctly at $M_\infty = 1.5$. The frequencies, though, are better predicted at $M_\infty = 2.5$.

C. Time-Averaged Pressure

The surface pressure distribution along the solid surfaces is measured once the flow has reached a state of self-sustained oscillation. The flow was judged to have reached a self-sustained oscillatory state once the p_{rms} and the tone frequencies were constant. The averaged surface pressure presented here is the averaged value over a 10 cycle period. In Fig. 14, both $M_\infty = 1.5$ and $M_\infty = 2.5$ results are shown. Comparison with the measured values shows good agreement. Encouragingly, the salient features are reproduced. These include the upstream effect of the cavity at $M_\infty = 1.5$, the effect of the large induced vortex near the trailing edge which gives rise to the pressure increase at the corner, and the effect of the shear layer impingement. Generally, the predicted pressure inside the cavity lies below the measured value, particularly on the upstream face of the cavity at $M_\infty = 1.5$. Overall, the prediction is good. This places confidence in the overall transient form drag coefficient prediction and the basic approach adapted in the study.

IV. Conclusions

A computational analysis is performed on flows over an $L/D = 3$ cavity at $M_\infty = 1.5$ and 2.5. The computation solves the mass-averaged Navier–Stokes equations as the fluid flow governing equations. Turbulence closure is achieved by implementing a k–ω model.

A self-sustained flow oscillatory state is achieved in the present computation. Both time-averaged and transient flowfields are studied. The shock and expansion wave patterns above the cavity are simulated which resemble the experimentally observed images. The wave emission is caused by the shear layer deflection, which in turn is associated with the vortex production and convection in the cavity. The correct wave pattern suggests the prediction of the dominant oscillatory modes by the current method. It is observed that the form drag coefficient varies with the shear layer impingement and mass ejection near the tailing edge of the cavity. Both positive and negative values are experienced in a complete cycle of oscillation. The predicted time-averaged pressure and sound pressure levels show a marked improvement over the previous studies. The time-averaged surface pressure agrees well with the measured value, which suggests that the present approach is sound. Further studies are needed to clarify the effects of the shear layer on high-frequency tones.

Acknowledgments

The study is supported by grants from the Nuffield Foundation and the Royal Society. The inviscid flux solver is adapted from the adaptive mesh refinement program provided by the Defence Research Agency. The author wishes to thank J. A. Edwards for his kind help and support.

References

[1]Krishnamurty, K., "Acoustic Radiation from Two-Dimensional Rectangular Cutouts in Aerodynamic Surfaces," NACA TN-3487, Aug. 1955.

[2]Charwat, A. F., Roos, J. N., Dewey, F. C., Jr., and Hitz, J. A., "An Investigation of Separated Flows—Part I: the Pressure Field," *Journal of the Aerospace Sciences*, Vol. 28, June 1961, pp. 457–470.

[3]Charwat, A. F., Dewey, F. C., Jr., Roos, J. N., and Hitz, J. A., "An Investigation of Separated Flows—Part II: Flow in the Cavity and Heat Transfer," *Journal of the Aerospace Sciences*, Vol. 28, July 1961, pp. 513–527.

[4]Rossiter, J. E., "Wind Tunnel Measurements on the Flow over Rectangular Cavities at Subsonic and Supersonic Speeds," Ministry of Aviation, Aeronautical Research Council, London, R&M 3438. Oct. 1964.

[5]Heller, H., Holmes, G., and Covert, E. E., "Flow Induced Pressure Oscillations in Shallow Cavities," AFFDL-TR-70-140, Wright–Patterson AFB, OH, Dec. 1970.

[6]Heller, H., and Bliss, D., "Aerodynamically Induced Pressure Oscillations in Cavities: Physical Mechanisms and Suppression Concepts," AFFDL-TR-74-133, Wright–Patterson AFB, OH, Feb. 1975.

[7]Zhang, X., and Edwards, J. A., "An Investigation of Supersonic Oscillatory Cavity Flows Driven by a Thick Shear Layer," *Aeronautical Journal*, Vol. 94, No. 940, 1990, pp. 355–364.

[8]Tam, C. K. W., and Block, P. J. W., "On the Tones and Pressure Oscillations Induced by Flow over Rectangular Cavities," *Journal of Fluid Mechanics*, Vol. 89, Pt. 2, Nov. 1978, pp. 373–399.

[9]Hankey, W. L., and Shang, J. S., "Analysis of Pressure Oscillation in an Open Cavity," *AIAA Journal*, Vol. 18, No. 8, 1980, pp. 892–898.

[10]Rizzetta, D. P., "Numerical Simulation of Supersonic Flow over a Three-Dimensional Cavity," *AIAA Journal*, Vol. 26, No. 7, 1988, pp. 799–807.

[11]Zhang, X., and Edwards, J. A., "Computational Analysis of Unsteady Cavity Flows Driven by Thick Shear Layers," *Aeronautical Journal*, Vol. 92, No. 919, 1988, pp. 365–374.

[12]Brailovskaya, I. Y., "A Difference Scheme for Numerical Solution of the Two-Dimensional Nonstationary Navier–Stokes Equations for a Compressible Flow," *Soviet Physics–Doklady*, Vol. 10, Pt. 2, Aug. 1965, pp. 107–110.

[13]Diewert, G. S., "Computation of Separated Transonic Turbulent Flows," *AIAA Journal*, Vol. 14, No. 6, 1974, pp. 735–740.

[14]Wilcox, D. C., "Reassessment of the Scale Determining Equation for Advanced Turbulence Models," *AIAA Journal*, Vol. 26, No. 11, 1988, pp. 1299–1310.

[15]Wilcox, D. C., "Dilatation-Dissipation Corrections for Advanced Turbulence Models," *AIAA Journal*, Vol. 30, No. 11, 1992, pp. 2639–2646.

[16]Roe, P., "Approximate Riemann Solvers, Parameter Vectors, and Difference Schemes," *Journal of Computational Physics*, Vol. 43, No. 2, 1981, pp. 357–372.

[17]Roe, P., "Characteristic-Based Schemes for the Euler Equations," *Annual Review of Fluid Mechanics*, Vol. 18, 1986, pp. 337–365.

[18]Quirk, J. J., "An Adaptive Grid Algorithm for Computational Shock Hydrodynamics," Ph.D. Thesis, College of Aeronautics, Cranfield Inst. of Technology, England, UK, Jan. 1991.

[19]Strang, G., "On the Construction and Comparison of Difference Schemes," *SIAM Journal on Numerical Analysis*, Vol. 5, No. 3, 1968, pp. 506–517.

[20]Osher, S., "Riemann Solvers, the Entropy Condition and Difference Approximations," *SIAM Journal on Numerical Analysis*, Vol. 21, No. 2, 1984, pp. 217–235.

[21]Roe, P. L., "Some Contributions to the Modelling of Discontinuous Flows," *Lectures in Applied Mathematics*, American Mathematical Society, Vol. 22, Pt. 2, 1985, pp. 163–193.

[22]Wilcox, D. C., "Turbulence Modelling for CFD," DCW Industries, Inc., La Cañada, CA, 1993.

[23]Zhang, X., and Edwards, J. A., "An Experimental Investigation of Supersonic Flow over Two Cavities in Tandem," *AIAA Journal*, Vol. 30, No. 5, 1992, pp. 1182–1190.